applied sciences

MDPI

Article

A Multi-Objective Optimization of 2D Materials Modified Surface Plasmon Resonance (SPR) Based Sensors: An NSGA II Approach

Pericle Varasteanu [1,2,*] and Mihaela Kusko [1]

[1] National Institute for Research and Development in Microtechnology (IMT-Bucharest), 126A Erou Iancu Nicolae Street, 077190 Voluntari, Romania; mihaela.kusko@imt.ro
[2] Faculty of Physics, University of Bucharest, 405 Atomistilor Street, 077125 Magurele, Romania
* Correspondence: pericle.varasteanu@imt.ro

Abstract: Modifying the structure of surface plasmon resonance based sensors by adding 2D materials has been proven to considerably enhance the sensor's sensitivity in comparison to a traditional three layer configuration. Moreover, a thin semiconductor film placed on top of the metallic layer and stacked together with 2D materials enhances even more sensitivity, but at the cost of worsening the plasmonic couplic strength at resonance (minimum level of reflectivity) and broadening the response. With each supplementary layer added, the complexity of optimizing the performance increases due to the extended parameter space of the sensor. This study focused on overcoming these difficulties in the design process of sensors by employing a multi-objective genetic algorithm (NSGA II) alongside a transfer matrix method (TMM) and, at the same time, optimizing the sensitivity to full width at half maximum (FWHM), and the reflectivity level at a resonance for a four layer sensor structure. Firstly, the thin semiconductor's refractive index was optimized to obtain the maximum achievable sensitivity with a narrow FWHM and a reflectivity level at a resonance of almost zero. Secondly, it was shown that refractive indices of barium titanate ($BaTiO_3$) and silicon (Si) are the closest to the optimal indices for the silver—graphene/WS_2 and MoS_2 modified structures, respectively. Sensitivities up to 302 deg/RIU were achieved by Ag–$BaTIO_3$–graphene/WS_2 configurations with an FWHM smaller than 8 deg and a reflectivity level less than 0.5% at resonance.

Keywords: SPR based sensors; NSGA II optimization; sensitivity enhancement

check for updates

Citation: Varasteanu, P.; Kusko, M. A Multi-Objective Optimization of 2D Materials Modified Surface Plasmon Resonance (SPR) Based Sensors: An NSGA II Approach. *Appl. Sci.* **2021**, *11*, 4353. https://doi.org/10.3390/app11104353

Academic Editor: Daniela Dragoman

Received: 21 April 2021
Accepted: 8 May 2021
Published: 11 May 2021

1. Introduction

The configurations first proposed by Otto [1] and Kretchmann and Raether [2] to couple incidence light to surface plasmon modes at a metal–air interface renewed the challenges and emerging direction in the area of sensors. Thus, in the 1980s, the successful achievement of both gas detection and biomolecular sensing based on surface plasmons in a Kretchmann configuration was reported [3]. At present, surface plasmon resonance (SPR) based sensors are an important part of different domains such as analytical chemistry, biology, and diagnostics due to their high sensitivity which eliminates the labeling process and could alter the properties of the molecules and also the possibility of real-time monitoring of the interactions involved in kinetic studies. The increased detection performance derives from the extremely sensitive reflectivity of the thin metal film with optical variations (refractive index changes) of the medium placed on one side of it. However, as the high sensing performance drastically degrades when low mass analytes are used [4], the simple SPR sensor configuration has been continually adjusted to allow single molecule detection [5], prenatal diagnostics [6], food safety [7] and temperature sensing [8].

It has been shown that by adding a thin semiconductor layer on top of the metal, the overall performance of a sensor can be improved [9]. Moreover, this film acts as a protective coating when silver is used as plasmonic metal, improving its chemical stability [10].

However, although the sensitivity is enhanced, in comparison to a classic structure, the response becomes broader as a result of the thickness of the dielectric and its inherent absorption [11]. This problem has been overcome using graphene monolayers with improved light absorption [12] that also increases the biological compatibility [13]. However, the semiconductor's thickness and the number of graphene monolayers have to be carefully chosen to attain a good performance. Newly emerging graphene 2D materials which are made up of transition metal dichalcogenide monolayers (TMDC), such as MoS_2, WS_2, etc., have also been utilized in SPR sensor design to improve their performance [11,14,15]. Similar to graphene monolayers, MoS_2 and WS_2 provide a high affinity for a wide range of target molecules due to their hydrophobic nature [16,17]. The biocompatibility of the 2D materials (Graphene, MoS_2 and WS_2) used here has been extensively studied in the literature [18–20]. Various biosensors and immunosensors with a great performance based on these 2D materials have been proposed such as: dopamine, ascorbic acid and uric acid detection sensors [21]; single strand DNA (ssDNA) interaction sensors [22]; and sensors used in the detection of prostate-specific antigens [23]. Furthermore, the main drawback of graphene coated sensors is that the increased overall absorption with the number of monolayers added, could be overcome by using these new materials as they show a high absorption for only one monolayer [24–26].

Recently, more complex configurations based on metal–semiconductor/2D material–metal–2D material [27] and even semiconductor–metal–dielectric–2D material contacts [28] have been developed. For these architectures, the conventional method of varying each layer's thickness has become almost impossible due to the size of the design space (i.e., thickness of the metallic layer, number of monolayers). Design optimization studies have been performed with promising results using algorithms that are inspired by nature, such as particle swarm optimization [29,30] or genetic algorithms [31]. Whereas genetic algorithms mimic natural evolution, the particle swarm optimization process is ispired by bird flock movements, and have been employed to further improve the graphene [31] or TMDC based SPR sensor's performance [32] or to discover new configurations regarding the plasmonic platform material [31].

Despite the recent successful implementation of genetic algorithms in the design process of SPR based sensors [26,31], there is still much room for improvement, due to their performance dependence on not only the sensitivity, but also the full width at half maximum (FWHM) or minimum level of reflectivity at resonance. To regulate all these parameters at the same time a multi-objective optimization must be perfomed on the sensor design. The non-dominated sorting genetic algorithm II (NSGA II) proposed by Deb [33] in 2002 can easily deal with multiple objectives, making it a suitable approach for improving the SPR sensor design. In 2014, the NSGA II was succesufuly applied to the optimization of a magneto-optical surface plasmon resonance sensor configuration using two objectives: the first was sensitivity, while the second was profiling the normalized sensor sensitivity against the thickness of a single layer [34].

This work is focused on the optimization of an SPR sensor architecture through the NSGA II algorithm, when a thin semiconductor layer and a 2D material, either graphene, MoS_2 or WS_2, are placed on top of the metallic layer in order to improve the detection performance. To find the best configurations, two test cases were analysed with the following objectives: (i) sensitivity and FWHM, and (ii) sensitivity, FWHM, and reflectivity level at resonance. Thus, the silver thickness, the number of 2D material monolayers and the semiconductor thickness were the parameters to be optimized. Moreover, the semiconductor refractive index was also considered a parameter in order to obtain the theoretical limit of the performance of these kinds of sensors. Finally, based on the optimized value of the refractive index for the hypothetical semiconductor, we propose standard materials with refractive indices close to the optimum values determined through simulations and we repeat the optimization process to obtain a fine adjustment of the sensor architecture, to facilitate further technological implementation.

2. Materials and Methods

The configuration of the SPR sensor emerged from the classical Kretchmann configuration (prism–metallic layer–sensing medium), where two additional layers, a thin semiconductor layer and a graphene/TMDC (MoS_2 or WS_2) monolayer, were stacked on top of the metallic layer, as shown in Figure 1.

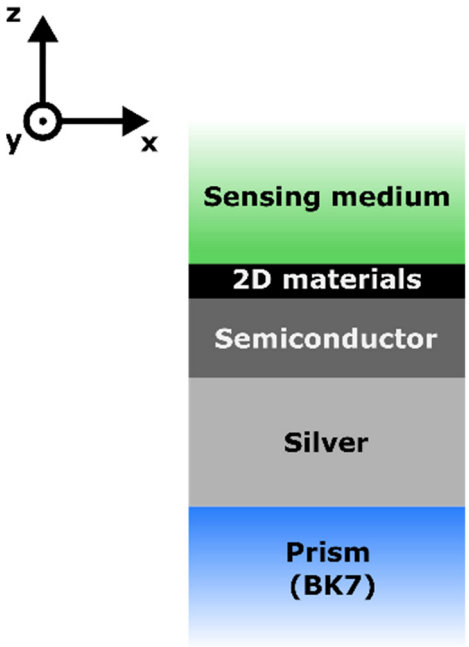

Figure 1. The proposed sensor configurations.

The material for the coupling prism was borosilicate-crown glass (BK7) with a refractive index calculated using the following equation:

$$n^2 - 1 = \frac{1.03961212\lambda^2}{\lambda^2 - 0.00600069867} + \frac{0.231792344\lambda^2}{\lambda^2 - 0.0200179144} + \frac{1.01046945\lambda^2}{\lambda^2 - 103.560653} \quad (1)$$

where λ is the incidence wavelength expressed in µm, and the dispersion parameters were taken from [35].

The layers were stacked on top of each other in the z-direction and dimensions for all layers in the x and y directions are considered infinite. The complex refractive index of the silver layer was calculated using the following equation [36]:

$$\widetilde{n}_{Ag} = \sqrt{1 - \frac{\lambda^2 \lambda_c}{\lambda_p^2(\lambda_c + i\lambda)}} \quad (2)$$

where λ is the incident radiation wavelength in µm, λ_c and λ_p are the collision and plasma wavelengths that have the values 1.7614×10^{-5} m and 1.4541×10^{-7} m, respectively.

The graphene monolayer thickness was considered 0.34 nm and the complex refractive index was computed with the following equation [37]:

$$\widetilde{n}_{Graphene} = 3 + \frac{iC_1\lambda}{3} \quad (3)$$

where C_1 has a value of 5.446 μm^{-1}.

The optical parameters and the thickness of one monolayer of TMDC are 5.0805 + 1.1724i and 0.65 nm for MoS_2 [24], and 4.8937 + 0.3123i and 0.8 nm for WS_2 [24], respectively.

The last layer from the configuration is the region where the biomolecular interactions (adsorption, DNA hybridization, etc.) take place, even though in an SPR classic configuration this layer is called the 'sensing medium'. The sensing medium's refractive index varied from 1.332 to 1.337 with a change of 0.005 RI (refractive index units).

It is worth mentioning that two approximations were made: (i) the quantum effects between graphene/TMDC monolayers were neglected, and, (ii) when more than two graphene/TMDC monolayers were stacked on top of each other the complex refractive index of the overall layer was considered the same as the one for one monolayer but with an increased thickness (N × monolayer thickness) [38].

The SPR sensor's response depends on two damping processes [39]: (i) the leakage radiation due to the interference phenomena resulting from the multiple interfaces, and (ii) the absorption loss due to the energy transfer between the incident photons and the metallic layer phonons.

A resonant energy transfer between incident radiation and surface plasmon polaritons (SPPs) appears by varying the angle of incidence, and, as a result, the resonance is seen as a sharp drop in reflectivity levels. Considering a classic three layer configuration, the equation for the resonance condition gives the angle at which the SPP wave is coupled with the incident radiation:

$$k_0 n_p \sin\theta = k_0 \sqrt{\frac{\varepsilon_s \varepsilon_m}{\varepsilon_d + \varepsilon_m}} \tag{4}$$

where k_0 is the incident light wavevector, n_p is the prism's refractive index, θ is the incidence radiation angle, and $\varepsilon_{s,m}$ represents the dielectric constants of the semiconductor and metal, respectively. The left-hand side of the equation is the propagation vector of light in the prism, whilst the right-hand side is the propagation vector of SPP from the metallic interface.

The sensor's sensitivity is defined as the displacement of the resonance angle ($\Delta\theta_{res}$) with the change of sensing medium's refractive index (Δn):

$$S = \frac{\Delta\theta_{res}}{\Delta n} \tag{5}$$

The optimization of the sensor configuration was performed using the non-dominated sorting genetic algorithm II (NSGA II) [33] together with the transfer matrix method [40], a ubiquitous tool in the design of surface plasmon resonance based sensors. A schematic presentation of the NSGA II implementation alongside the TMM is shown in Figure 2.

The objectives of the problem were to: (i) maximize sensitivity (i.e., even though the algorithm is solving a minimization problem, the sensitivity is maximized by minimizing its negative); (ii) minimize the FWHM, which is related to the overall absorption in the sensor structure (i.e., when the light absorption in the metallic layer and subsequent layers increases, the reflectivity curve broadens); and (iii) minimize level of reflectivity at resonance (assuring a strong coupling between the surface plasmons and the incident light [41]).

First, an initial population of 500 random configurations is generated, then the TMM computes the responses (e.g., minimum level of reflectivity, sensitivity, and FWHM) of each configuration. Second, NSGA II ranks the configurations based on their performance (nondomination) and then applies the selection to choose configurations that produce the offspring structures. Crossover (int or real SBX [42]) and mutation (int and real Polynomial [42]) operations are applied to create the offspring population. The two populations (initial and newly created after aplying genetic operations) are then combined into one set. Third, TMM computes the offspring population's responses, then sorts the configurations based on their performance (nondomination) on different fronts to select which configuration is transferred to the new generation. Solutions from the last front are then compared based on the crowding distance in order to select which configuration should be transferred to the new final population. Because NSGA II is an elitist multi-objective genetic algorithm [33], the best solutions are preserved through generations. The final

population becomes the initial population from step 1 and the process is repeated until the termination criterion is met. It is worth mentioning that in multi-objective optimization, where the objectives compete with each other, solutions might exist where one objective cannot be improved without degrading the others [43], therefore, a set of optimal configurations can be found. For example, configurations with a greatly enhanced sensitivity could be generated, but they have an FWHM close to the constraint of 10 deg and, conversely, a solution with a narrow FWHM, but a sensitivity close to the imposed lower limit of 200 deg/RIU. Table 1 summarises the sensor parameters considered to be optimized.

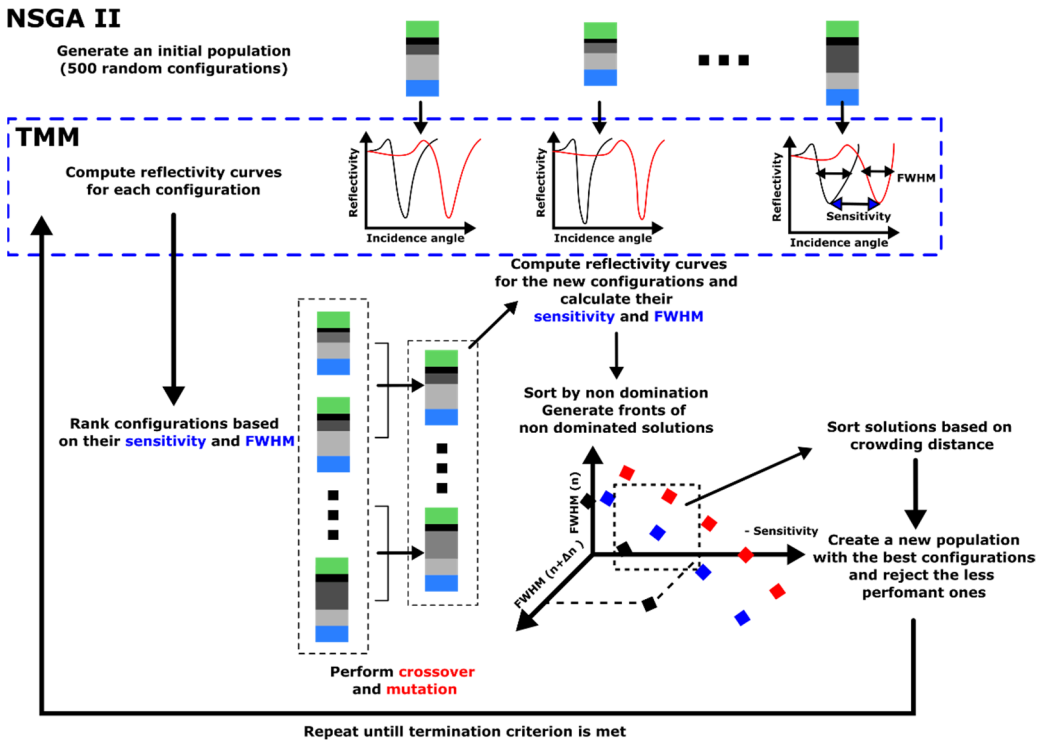

Figure 2. Schematics of the implementation of the NGSA II algorithm alongside TMM.

Table 1. Parameter space, objectives and constraints used in NGSA II algortihm.

L.N.	Parameters	Parameter Space	Objectives	Constraints
1	Ag thickness	0–100 nm	-Sensitivity	<−200 deg/RIU
2	Semiconductor's thickness	0–50 nm	FWHM	<10 deg
3	Semiconductor's refractive index	1.34–4	Reflectivity at resonance	<1%
4	No. of 2D material monolayers	1–10 L		

It is worth mentioning that in order to decrease the parameter space, a mixed problem was solved, where the metallic thickness, semiconductor thickness, and the number of monolayers were considered integer values, while the semiconductor refractive index was considered real. The TMM code was written in Python [44] and for the optimization, the 'pymoo' framework [45] was employed.

3. Results

First, the NSGA II was used to optimize the metal thickness, the semiconductor thickness and the refractive index, and the number of graphene/TMDC monolayers without minimization of the reflectivity level. The reflectivity curves for the optimized configurations with the best sensitivity and narrowest FWHM are shown in Figure 3. The black line

represents the response of the configurations that present an enhanced sensitivity, whilst the red line indicates the configurations with narrow reflectivity curves (small FWHM). The convergence plots of objectives and layers can be found in Supplementary Information Figure S1.

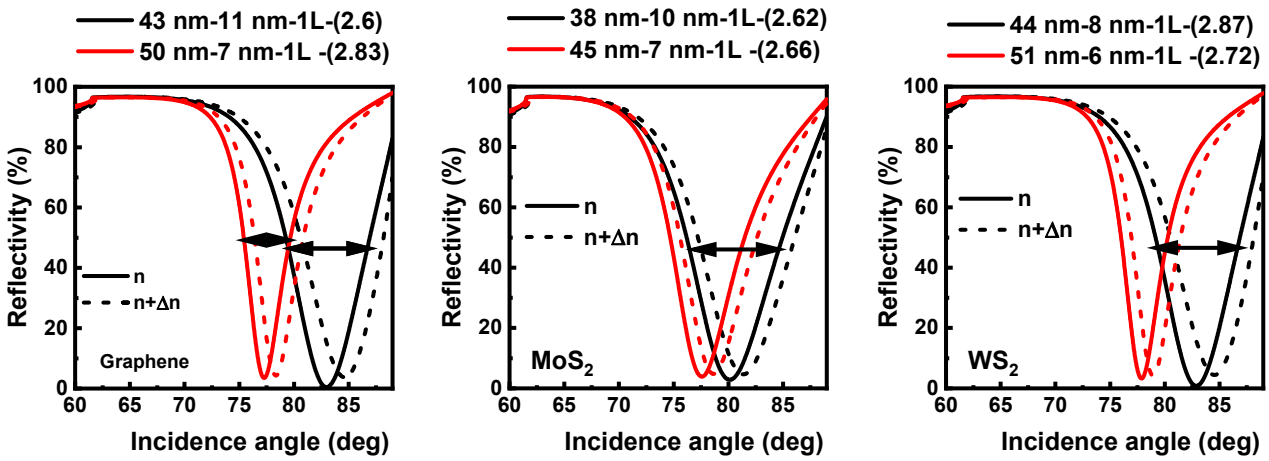

Figure 3. Reflectivity curves for the optimized semiconductor refractive index: the black line shows the high sensitivity configurations, the red line shows the narrow FWHM configurations, the dashed lines shows the sensor's response for $n + \Delta n$, $\Delta n = 0.005$.

The results clearly show that, whereas in order to enhance sensitivity, the thickness of the silver layer must be decreased and the semiconductor layer must be increased, conversely, for a smaller FWHM, the thickness of the silver must be increased and the thickness of the semiconductor decreased. The differences in sensitivity and FWHM between the two types of structure (sensitivity enhanced configuration and small FWHM configuration) are shown in Table 2. (The convergence plots of layers and objectives can be found in Figure S1 and additional configurations together with the sensitivity and FWHM can be found in Figure S2 and Table S1 in the Supplementary Information).

Table 2. Configurations with the optimal dielectric refractive index for which the sensitivity is enhanced and FHWM is lowered.

L.N.	Material	Configuration Metal–Semic.–2D Mat.–(n_{diel})	Sensitivity (deg/RIU)	FWHM (deg)
1	Graphene	43 nm–11 nm–1 L (2.6)	331	7.1
2		50 nm–7 nm–1 L (2.83)	202	3.9
3	MoS_2	38 nm–10 nm–1 L (2.62)	258	8.9
4		45 nm–7 nm–1 L (2.66)	205	6
5	WS_2	44 nm–8 nm–1 L (2.87)	333	7
6		51 nm–6 nm–1 L (2.72)	206	3.7

The combination of the imaginary part of the refractive index and the thickness of the 2D materials plays an important role in the SPR response. Due to the higher imaginary part of the MoS_2 refractive index that induces an additional loss, the structures modified with MoS_2 present a broader reflectivity curve and also a smaller sensitivity in comparison to the other configurations. Thus, the highest sensitivity achieved is 258 deg/RIU which is about 60 deg/RIU less than the sensitivity obtained for graphene and WS_2 structures. Looking at the FWHM, the structure containing MoS_2 has the narrowest FWHM of 5.8 deg. and a sensitivity of 198 deg/RIU, while WS_2 and graphene based structures have sensitivities around 204 deg/RIU, and a FWHM of 3.4 deg. and 3.6 deg., respectively. Configurations containing the WS_2 monolayers exhibit a slightly higher sensitivity and also a narrower reflectivity curve in comparison to the graphene modified monolayers, mainly due to its

smaller imaginary part of the refractive index, i.e., 333 deg/RIU with a 7 deg FWHM in comparison with 331 deg/RIU and 7.1 deg FWHM. Because the end goal is to maximize sensitivity, the discussion will be restricted to the structures that enhance it. From Table 2 it can be observed that the thin semiconductor's refractive index is 2.6 for the graphene, 2.62 for the MoS_2 and 2.66 for the WS_2. Among all materials that have been already utilized as top layers in SPR based sensors, $BaTiO_3$, having a refractive index of 2.405 [46], is the best candidate for this layer in the proposed sensor configurations.

To verify if $BaTiO_3$ could really improve the sensing performance of the modified sensors, an additional set of optimizations was performed, to find the optimum thickness of the $BaTiO_3$ layer, using the same objectives and constraints as in the previous run. The convergence plots of layers and objectives can be found in Figure S3 and additional configurations together with the sensitivity and FWHM can be found in Figure S4 and Table S2 in Supplementary Information. The reflectivity curves of the most sensitive configurations containing $BaTiO_3$ can be seen in Figure 4.

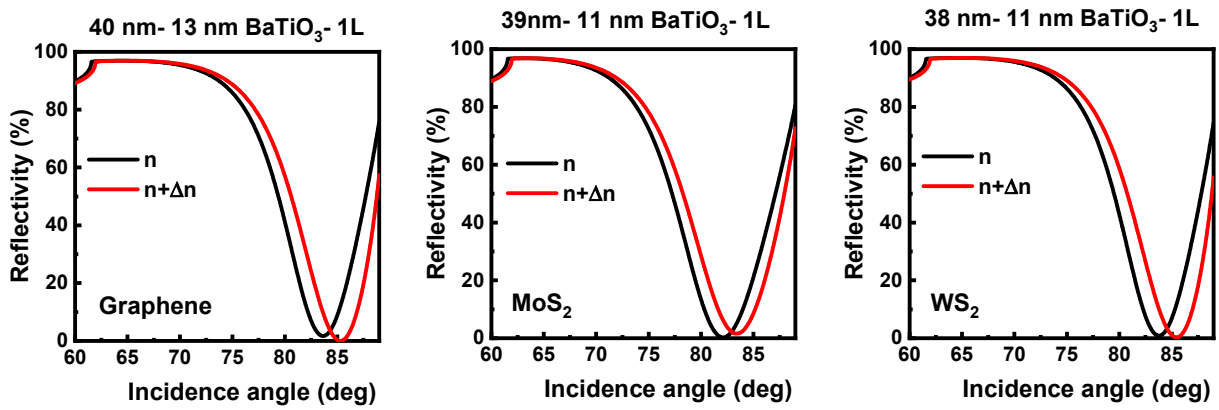

Figure 4. Reflectivity curves for the optimized structures containing the $BaTiO_3$ as a dielectric: black line shows the response for n = 1.332, the red line shows the response for $n + \Delta n$ with Δn = 0.005.

Table 3 demonstrates that the sensitivities obtained for all structures modified with $BaTiO_3$ are very close to those with the optimal refractive index, with the maximum difference in sensitivity being 9 deg/RIU for the configuration with MoS_2. Similarly, the FWHM values also change, and the FWHM value corresponding to MoS_2 with the optimal material refractive index is increased from 8.9 to 9.2 deg. The highest sensitivities, 330 deg/RIU and 325 deg/RIU, were obtained for the structures with graphene and WS_2, respectively. As in previous optimization studies, several solutions were found with a lower sensitivity of 200 deg/RIU, but with narrower reflectivity curves (<6 deg). Despite the enhanced performance of these structures, since the minimum level of reflectivity reaches a value of 5%, it is considered too high because of the inherent variations in the layer thickness during the fabrication process.

Table 3. Optimized configurations with $BaTiO_3$ for which the sensitivity is enhanced.

L.N.	Material	Configuration Metal–Semic.–2D Mat.	Sensitivity (deg/RIU)	FWHM (deg)
1	Graphene	40 nm–13 nm–1 L	330	7.1
2	MoS_2	39 nm–11 nm–1 L	249	9.2
3	WS_2	38 nm–11 nm–1 L	325	8

Further, to eliminate the potential variations that could affect the sensor performance under realistic conditions, a new set of optimizations was performed, where the minimum level of reflectivity was introduced as an objective and constrained to be smaller than 1%. The reflectivity curves can be seen in Figure 5 and the performance determined for

each configuration are presented in Table 4. In this case, there are three types of optimal configurations: one that improves sensitivity (black line), a second that narrows the FWHM (red line), and a third that minimizes the reflectivity level at resonance (blue line). The convergence plots of the layers and the objectives can be found in Figure S5. Additional configurations, together with the sensitivity and FWHM, can be found in Figure S3 and Table S6 in the Supplementary Information.

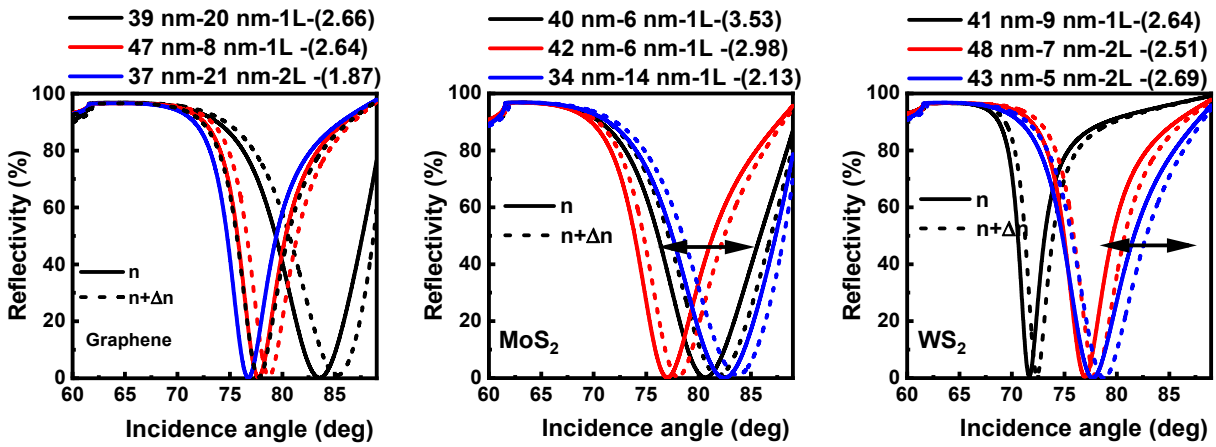

Figure 5. Reflectivity curves for the optimized semiconductor refractive index: the black line shows the sensitivity enhanced configurations, the red line shows the FWHM narrowing structures, the blue line shows the configurations with the minimum level of reflectivity at resonance minimized, the dashed line shows the sensor's response for $n + \Delta n$.

Table 4. Configurations with the optimal refractive index, for which the sensitivity is enhanced, FHWM is narrowed and the reflectivity level at resonance is minimised.

L.N.	Material	Configuration Metal–Semiconductor–2D Mat. ($n_{semiconductor}$)	Sensitivity (deg/RIU)	FWHM (deg)
1		40 nm–11 nm–1 L (2.66)	325	7.1
2	Graphene	47 nm–8 nm–1 L (2.64)	200	4.6
3		37 nm–21 nm–2 L (1.87)	212	7
4		40 nm–6 nm–1 L (3.53)	256	9.3
5	MoS_2	42 nm–6 nm–1 L (2.98)	200	7.4
6		34 nm–14 nm–1 L (2.13)	254	9.2
7		41 nm–9 nm–1 L (2.64)	314	7.9
8	WS_2	48 nm–7 nm–2 L (2.51)	208	4.6
9		43 nm–5 nm–2 L (2.69)	212	7

From these results, it can be noted that adding the minimum level of reflectivity as an additional objective led to a slightly decreased sensitivity in comparison to the one obtained initially. Thus, the highest sensitivity for the graphene modified structure when the reflectivity level was not optimized was 330 deg/RIU, but now it is 325 deg/RIU. As in the first case, the same trend was observed: where to enhance the sensitivity, the metallic layer thickness should be decreased and to reduce the FWHM, the metallic layer thickness should be increased. Accordingly, for the MoS_2 structure, the refractive index of the top layer that maximizes sensitivity is 3.53, and, consequently, silicon is the the best candidate to accomplish the requirements of the hypothethical material.

Furthermore, considering the value of the refractive index for which the structure's sensitivity is greatly enhanced, the fourth set of optimizations was run, where the metal thickness, the semiconductor thickness, and the number of 2D material monolayers were considered as parameters. $BaTiO_3$ was selected for the graphene and WS_2 configurations was chosen because its refractive index was closest to the optimal levels (2.66 for graphene and 2.64 for WS_2) [47], while silicon for MoS_2 based structure. The reflectivity curves can

be seen in Figure 6 and the performance determined for each configuration are presented in Table 5. The convergence plots of these layers and objectives can be found in Figure S7 and additional configurations together with the sensitivity and FWHM can be found in Figure S8 and Table S4 in the Supplementary Information.

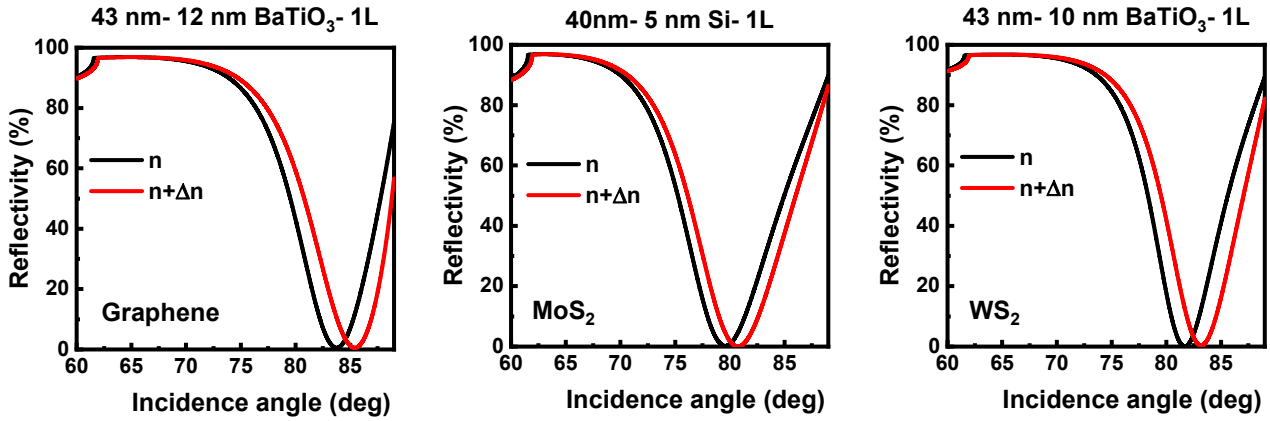

Figure 6. Reflectivity curves for the optimized structures with $BaTiO_3$ and Si.

Table 5. Configurations with the $BaTiO_3$ and Si for which the sesntivity is enhanced.

L.N.	Material	Configuration Metal–Semic.–2D Mat.	Sensitivity (deg/RIU)	FWHM (deg)
1	Graphene	43 nm–12 nm–1 L; ($BaTiO_3$)	302	7.1
2	MoS_2	39 nm–5 nm–1 L; (Si)	232	9.4
3	WS_2	43 nm–10 nm–1 L; ($BaTiO_3$)	302	8

The refractive index of silicon was calculated using the following formula [48]:

$$n_{SI} = A + A_1 e^{-\frac{\lambda}{t_1}} + A_2 e^{-\frac{\lambda}{t_2}} \quad (6)$$

where A = 0.344904, A_1 = 2271.88813, A_2 = 3.39538, $t_1 = 0.058304$, $t_2 = 0.30384$ and λ is the wavelength. Because it was shown that polycristaline silicon with a thickness of 10 nm would not induce a strong absorption in a visible spectrum [49], the extinction coefficient was neglected.

In this case, the minimum level of reflectivity strongly influences the sensitivity. Thus, if the graphene based structure sensitivity was 330 deg/RIU with a minimum level of reflectivity at 4%, in this case, the sensitivity is decreased to 302 deg/RIU, but the reflectivity level at resonance is smaller than 0.5%. Similarly, for the WS_2 based configuration, sensitivity decreased from 325 deg/RIU to 302 deg/RIU and for the MoS_2 based configuration it decreased from 255 deg/RIU to 232 deg/RIU. It is worth mentioning that the FWHM is not improved nor altered.

A quantitative comparison of the recent literature with the results obtained in this work is presented in Table 6. Only the configurations based on the BK7 prism and silver as a plasmonic platform were compared.

It can be observed that an enhanced sensitivity is obtained by adding a thin semiconductor film on top of the metallic layer, in comparison to configurations that uses different combinations of 2D materials [50] (i.e., structures with black phosphprus (BP) and Graphene/MoS_2/WS_2). It is worth mentioning that by employing NSGA II together with the TMM, the $BaTiO_3$ thin film greatly improves the performance for the structure consisting in Ag-graphene [36] or ZnO–Ag–2D materials [28] with no prior information about its refractive index. Moreover, a structure with an almost 50 deg/RIU improvement in sensitivity was obtained.

Table 6. Comparison of configurations found in the literature based on BK7 prism and graphene/2D materials.

L.N.	Configuration	Sensitivity (deg/RIU)	Refractive Index Range	Ref.
1	BK7–ZnO–Ag–$BaTiO_3$–graphene	157	1.330–1.350	[28]
2	BK7–BP–graphene	217	1.330–1.335	[50]
3	BK7–BP–MoS_2	218	1.330–1.335	[50]
4	BK7–BP–WS_2	237	1.330–1.335	[50]
5	BK7–ZnO–Ag–$BaTiO_3$–MoS_2	174	1.330–1.350	[28]
6	BK7–ZnO–Ag–$BaTiO_3$–WS_2	180	1.330–1.350	[28]
7	BK7–Ag–$BaTiO_3$–graphene	257	1.338–1.348	[36]
8	BK–Ag–$BaTiO_3$–graphene	302	1.332–1.337	This work
9	BK7–Ag–Si–MoS_2	232	1.332–1.337	This work
10	BK7–Ag–$BaTiO_3$–WS_2	302	1.332–1.337	This work

4. Conclusions

In this study, a multi-objective optimization algorithm, NSGA II, was employed alongside a TMM to find the SPR based sensor configurations that could present an enhanced sensing performance. The theoretical limit of maximal sensitivity with narrow FWHM and a reflectivity level at a resonance smaller than 1% was achieved for structures modified with a thin material placed on top of silver and graphene, MoS_2 or WS_2. Moreover, it was shown that the optimal refractive index values for the thin top layer were close to the levels of standard semiconductors, connecting our numerical analyses to real architectures. Sensitivities up to 302 deg/RIU were achieved for the structures containing 43 nm silver, 12 nm $BaTiO_3$ and one monolayer of graphene and 43 nm silver, 10 nm $BaTiO_3$ and one monolayer of WS_2, respectively. From our extensive analysis on the effects of additional layers on the sensing performance of SPR based sensors we can draw the conclusion that multi-objective optimization employed together with the TMM could pave the way for the next ultrasensitive SPR based sensors providing solutions that can be easy to implement.

Supplementary Materials: The following are available online at https://www.mdpi.com/article/10.3390/app11104353/s1, Figure S1: Convergence plots for the Ag–Semicondcutor–2D material–Sensing medium ($n_{semiconductor}$) configuration with -sensitivity and FWHM as objectives; Left column: the layer thicknesses convergence and right column: the objectives, Figure S2: Reflectivity curves for the Ag–Semicondcutor–2D material–Sensing medium ($n_{semiconductor}$) configuration, Table S1: Additional configurations for the structure: Ag-semiconductor-2D material-Sensing medium, Figure S3: Convergence plots for the Ag–$BaTiO_3$–2D material–Sensing medium configuration with -sensitivity and FWHM as objectives; Left column: the layer thickness convergence and right column: the objectives convergence, Figure S4: Reflectivity curves for the Ag–$BaTiO_3$–2D material–Sensing medium configuration, Table S2: Additional configurations for the structure: Ag-$BaTiO_3$-2D material-Sensing medium, Figure S5: Convergence plots for the Ag–Semicondcutor–2D material–Sensing medium ($n_{semiconductor}$) configuration with -sensitivity, FWHM, and minimum level of reflectivity as objectives; Left column: the layer thickness convergence and right column: the objectives convergence, Figure S6: Reflectivity curves for the Ag–Semicondcutor–2D material–Sensing medium ($n_{semiconductor}$) configuration with -sensitivity, FWHM, and minimum level of reflectivity as objectives, Table S3: Additional configurations for the structure: Ag–Semiconductor–2D material–Sensing medium, Figure S7: Convergence plots for the Ag–$BaTiO_3$/Si–2D material–Sensing medium configuration with -sensitivity, FWHM, and minimum level of reflectivity as objectives; Left column: the layer thickness convergence and right column: the objectives convergence, Figure S8: Reflectivity curves for the Convergence plots for the Ag–$BaTiO_3$/Si–2D material–Sensing medium configuration with -sensitivity, FWHM, and minimum level of reflectivity as objectives, Table S4: Additional configurations for the structure: Ag–$BaTiO_3$–2D material–Sensing medium.

Author Contributions: Conceptualization, P.V., writing—original draft preparation, P.V.; writing—review and editing, P.V. and M.K., supervision M.K. Both authors have read and agreed to the published version of the manuscript.

Funding: Financial support was provided by the Core Program PN 1916/2019 MICRO-NANO-SIS PLUS/08.02.2019 and PN-III-P1-1.2-PCCDI-2017-0820—Project no. 1, funded by MCI.

Institutional Review Board Statement: Not applicable.

Conflicts of Interest: The authors declare no conflict of interest.

References

1. Otto, A. Excitation of nonradiative surface plasma waves in silver by the method of frustrated total reflection. *Z. Phys.* **1968**, *216*, 398–410. [CrossRef]
2. Kretschmann, E.; Raether, H. Radiative Decay of Non Radiative Surface Plasmons Excited by Light. *Z. Nat. Sect. A J. Phys. Sci.* **1968**, *23*, 2135–2136. [CrossRef]
3. Liedberg, B.; Nylander, C.; Lunström, I. Surface plasmon resonance for gas detection and biosensing. *Sens. Actuators* **1983**, *4*, 299–304. [CrossRef]
4. Kabashin, A.V.; Evans, P.; Pastkovsky, S.; Hendren, W.; Wurtz, G.A.; Atkinson, R.; Pollard, R.; Podolskiy, V.A.; Zayats, A.V. Plasmonic nanorod metamaterials for biosensing. *Nat. Mater.* **2009**, *8*, 867–871. [CrossRef] [PubMed]
5. Taylor, A.B.; Zijlstra, P. Single-Molecule Plasmon Sensing: Current Status and Future Prospects. *ACS Sens.* **2017**, *2*, 1103–1122. [CrossRef]
6. Breveglieri, G.; Bassi, E.; Carlassara, S.; Cosenza, L.C.; Pellegatti, P.; Guerra, G.; Finotti, A.; Gambari, R.; Borgatti, M. Y-chromosome identification in circulating cell-free fetal DNA using surface plasmon resonance. *Prenat. Diagn.* **2016**, *36*, 353–361. [CrossRef]
7. Piliarik, M.; Párová, L.; Homola, J. High-throughput SPR sensor for food safety. *Biosens. Bioelectron.* **2009**, *24*, 1399–1404. [CrossRef]
8. Ibrahim, J.; Al Masri, M.; Verrier, I.; Kampfe, T.; Veillas, C.; Celle, F.; Cioulachtjian, S.; Lefèvre, F.; Jourlin, Y. Surface plasmon resonance based temperature sensors in liquid environment. *Sensors* **2019**, *19*, 3354. [CrossRef]
9. Kuttge, M.; Vesseur, E.J.R.; Verhoeven, J.; Lezec, H.J.; Atwater, H.A.; Polman, A. Loss mechanisms of surface plasmon polaritons on gold probed by cathodoluminescence imaging spectroscopy. *Appl. Phys. Lett.* **2008**, *93*, 23–26. [CrossRef]
10. Wang, G.; Wang, C.; Yang, R.; Liu, W.; Sun, S. A sensitive and stable surface plasmon resonance sensor based on monolayer protected silver film. *Sensors* **2017**, *17*, 2777. [CrossRef]
11. Zeng, S.; Hu, S.; Xia, J.; Anderson, T.; Dinh, X.Q.; Meng, X.M.; Coquet, P.; Yong, K.T. *Graphene-MoS2 Hybrid Nanostructures Enhanced Surface Plasmon Resonance Biosensors*; Elsevier B.V.: Amsterdam, The Netherlands, 2015; Volume 207, ISBN 0060006986.
12. Choi, S.H.; Kim, Y.L.; Byun, K.M. Graphene-on-silver substrates for sensitive surface plasmon resonance imaging biosensors. *Opt. Express* **2011**, *19*, 458. [CrossRef]
13. Liao, C.; Li, Y.; Tjong, S.C. Graphene nanomaterials: Synthesis, biocompatibility, and cytotoxicity. *Int. J. Mol. Sci.* **2018**, *19*, 3564. [CrossRef]
14. Zhao, X.; Huang, T.; Ping, P.S.; Wu, X.; Huang, P.; Pan, J.; Wu, Y.; Cheng, Z. Sensitivity enhancement in surface plasmon resonance biochemical sensor based on transition metal dichalcogenides/graphene heterostructure. *Sensors* **2018**, *18*, 2056. [CrossRef]
15. Han, L.; Chen, Z.; Huang, T.; Ding, H.; Wu, C. Sensitivity Enhancement of Ag-ITO-TMDCs-Graphene Nanostructure Based on Surface Plasmon Resonance Biosensors. *Plasmonics* **2019**. [CrossRef]
16. Xiao, M.; Chandrasekaran, A.R.; Ji, W.; Li, F.; Man, T.; Zhu, C.; Shen, X.; Pei, H.; Li, Q.; Li, L. Affinity-Modulated Molecular Beacons on MoS2 Nanosheets for MicroRNA Detection. *ACS Appl. Mater. Interfaces* **2018**, *10*, 35794–35800. [CrossRef]
17. Chen, J.; Gao, C.; Mallik, A.K.; Qiu, H. A WS2 nanosheet-based nanosensor for the ultrasensitive detection of small molecule-protein interaction via terminal protection of small molecule-linked DNA and Nt.BstNBI-assisted recycling amplification. *J. Mater. Chem. B* **2016**, *4*, 5161–5166. [CrossRef]
18. Bolotsky, A.; Butler, D.; Dong, C.; Gerace, K.; Glavin, N.R.; Muratore, C.; Robinson, J.A.; Ebrahimi, A. Two-Dimensional Materials in Biosensing and Healthcare: From in Vitro Diagnostics to Optogenetics and beyond. *ACS Nano* **2019**, *13*, 9781–9810. [CrossRef]
19. Li, S.; Ma, L.; Zhou, M.; Li, Y.; Xia, Y.; Fan, X.; Cheng, C.; Luo, H. New opportunities for emerging 2D materials in bioelectronics and biosensors. *Curr. Opin. Biomed. Eng.* **2020**, *13*, 32–41. [CrossRef]
20. Wen, W.; Song, Y.; Yan, X.; Zhu, C.; Du, D.; Wang, S.; Asiri, A.M.; Lin, Y. Recent advances in emerging 2D nanomaterials for biosensing and bioimaging applications. *Mater. Today* **2018**, *21*, 164–177. [CrossRef]
21. Qi, S.; Zhao, B.; Tang, H.; Jiang, X. Determination of ascorbic acid, dopamine, and uric acid by a novel electrochemical sensor based on pristine graphene. *Electrochim. Acta* **2015**, *161*, 395–402. [CrossRef]
22. Zhou, C.; Zou, H.; Li, M.; Sun, C.; Ren, D.; Li, Y. Fiber optic surface plasmon resonance sensor for detection of E. coli O157:H7 based on antimicrobial peptides and AgNPs-rGO. *Biosens. Bioelectron.* **2018**, *117*, 347–353. [CrossRef]
23. Sajid, M.; Osman, A.; Siddiqui, G.U.; Kim, H.B.; Kim, S.W.; Ko, J.B.; Lim, Y.K.; Choi, K.H. All-printed highly sensitive 2D MoS2 based multi-reagent immunosensor for smartphone based point-of-care diagnosis. *Sci. Rep.* **2017**, *7*, 1–11. [CrossRef]
24. Singh, S.; Singh, P.K.; Umar, A.; Lohia, P.; Albargi, H.; Castañeda, L.; Dwivedi, D.K. 2D nanomaterial-based surface plasmon resonance sensors for biosensing applications. *Micromachines* **2020**, *11*, 779. [CrossRef]
25. Jena, S.C.; Shrivastava, S.; Saxena, S.; Kumar, N.; Maiti, S.K.; Mishra, B.P.; Singh, R.K. Surface plasmon resonance immunosensor for label-free detection of BIRC5 biomarker in spontaneously occurring canine mammary tumours. *Sci. Rep.* **2019**, *9*, 1–12. [CrossRef]

26. Lin, Z.; Chen, S.; Lin, C. Sensitivity improvement of a surface plasmon resonance sensor based on two-dimensional materials hybrid structure in visible region: A theoretical study. *Sensors* **2020**, *20*, 2445. [CrossRef]
27. Xu, Y.; Ang, Y.S.; Wu, L.; Ang, L.K. High sensitivity surface plasmon resonance sensor based on two-dimensional MXene and transition metal dichalcogenide: A theoretical study. *Nanomaterials* **2019**, *9*, 165. [CrossRef]
28. Kumar, A.; Yadav, A.K.; Kushwaha, A.S.; Srivastava, S.K. A comparative study among WS2, MoS2 and graphene based surface plasmon resonance (SPR) sensor. *Sens. Actuators Rep.* **2020**, *2*, 100015. [CrossRef]
29. Amoosoltani, N.; Zarifkar, A.; Farmani, A. Particle swarm optimization and finite-difference time-domain (PSO/FDTD) algorithms for a surface plasmon resonance-based gas sensor. *J. Comput. Electron.* **2019**, *18*, 1354–1364. [CrossRef]
30. Sun, Y.; Cai, H.; Wang, X.; Zhan, S. Optimization methodology for structural multiparameter surface plasmon resonance sensors in different modulation modes based on particle swarm optimization. *Opt. Commun.* **2019**, *431*, 142–150. [CrossRef]
31. Lin, C.; Chen, S. Design of highly sensitive guided-wave surface plasmon resonance biosensor with deep dip using genetic algorithm. *Opt. Commun.* **2019**, *445*, 155–160. [CrossRef]
32. Vaz, W.S. Multiobjective optimization of a residential grid-tied solar system. *Sustainability* **2020**, *12*, 8648. [CrossRef]
33. Deb, K.; Member, A.; Pratap, A.; Agarwal, S.; Meyarivan, T. A Fast and Elitist Multiobjective Genetic Algorithm: NSGA-II. *IEEE Trans. Evol. Comput.* **2002**, *6*, 182–197. [CrossRef]
34. Pellegrini, G.; Mattei, G. High-Performance Magneto-Optic Surface Plasmon Resonance Sensor Design: An Optimization Approach. *Plasmonics* **2014**, *9*, 1457–1462. [CrossRef]
35. SCHOTT Optical Class Data Sheets. 2019. Available online: https://www.schott.com/en-us (accessed on 20 April 2021).
36. Sun, P.; Wang, M.; Liu, L.; Jiao, L.; Du, W.; Xia, F.; Liu, M.; Kong, W.; Dong, L.; Yun, M. Sensitivity enhancement of surface plasmon resonance biosensor based on graphene and barium titanate layers. *Appl. Surf. Sci.* **2019**, *475*, 342–347. [CrossRef]
37. Bruna, M.; Borini, S. Optical constants of graphene layers in the visible range. *Appl. Phys. Lett.* **2009**, *94*. [CrossRef]
38. Varasteanu, P. Transition Metal Dichalcogenides/Gold-Based Surface Plasmon Resonance Sensors: Exploring the Geometrical and Material Parameters. *Plasmonics* **2020**, *15*, 243–253. [CrossRef]
39. Raether, H.; Hohler, G.; Niekisch, E.A. Surface Plasmons on Smooth and Rough Surfaces and on Gratings. *Springer Tracts Mod. Phys.* **1988**, *111*, 136.
40. Shalabney, A.; Abdulhalim, I. Electromagnetic fields distribution in multilayer thin film structures and the origin of sensitivity enhancement in surface plasmon resonance sensors. *Sens. Actuators A Phys.* **2010**, *159*, 24–32. [CrossRef]
41. Wissmann, P.; Finzel, H.U. *Springer Tracts in Modern Physics: Introduction*; Springer: New York, NY, USA, 2007; Volume 223, ISBN 3540484884.
42. Deb, K.; Sindhya, K.; Okabe, T. Self-adaptive simulated binary crossover for real-parameter optimization. In Proceedings of the 9th Annual Conference on Genetic and Evolutionary Computation, London, UK, 7–11 July 2007; pp. 1187–1194. [CrossRef]
43. Kim, K.-Y.; Jung, J. Multiobjective optimization for a plasmonic nanoslit array sensor using Kriging models. *Appl. Opt.* **2017**, *56*, 5838. [CrossRef]
44. Van Rossum, G.; Drake, F.L. *Python 3 Reference Manual*; CreateSpace: Scotts Valley, CA, USA, 2009; ISBN 1441412697.
45. Blank, J.; Deb, K. Pymoo: Multi-Objective Optimization in Python. *IEEE Access* **2020**, *8*, 89497–89509. [CrossRef]
46. Fouad, S.; Sabri, N.; Jamal, Z.A.Z.; Poopalan, P. Surface plasmon resonance sensor sensitivity enhancement using gold-dielectric material. *Int. J. Nanoelectron. Mater.* **2017**, *10*, 147–156.
47. Wemple, S.H.; Didomenico, M.; Camlibel, I. Dielectric and optical properties of melt-grown $BaTiO_3$. *J. Phys. Chem. Solids* **1968**, *29*, 1797–1803. [CrossRef]
48. Palik, E.D. *Handbook of Optical Constants of Solids*; Academic Press: Cambridge, MA, USA, 1998; Volume 3.
49. Mirshafieyan, S.S.; Guo, J. Silicon colors: Spectral selective perfect light absorption in single layer silicon films on aluminum surface and its thermal tunability. *Opt. Express* **2014**, *22*, 31545. [CrossRef] [PubMed]
50. Wu, L.; Guo, J.; Wang, Q.; Lu, S.; Dai, X.; Xiang, Y.; Fan, D. Sensitivity enhancement by using few-layer black phosphorus-graphene/TMDCs heterostructure in surface plasmon resonance biochemical sensor. *Sens. Actuators B Chem.* **2017**, *249*, 542–548. [CrossRef]